Physical properties of fluorides barium and calcium nanopowders produced by the pulsed electron beam evaporation method

IOP Conf. Series: Journal of Physics: Conf. Series **1115** (2018) 032092 doi:10.1088/1742-6596/1115/3/032092

Physical properties of fluorides barium and calcium nanopowders produced by the pulsed electron beam evaporation method

S Yu Sokovnin[1,2], V G Il`ves[2], M G Zuev[1,3] and M A Uimin[1,4]

[1]Ural Federal University, 19 Mira Str., Yekaterinburg, 620002, Russia
[2]Institute of Electrophysics UB RAS, 106 Amundsen Str., Yekaterinburg, 620016, Russia
[3]Institute of Solid State Chemistry UB RAS, 91 Pervomaiskaya Str., Yekaterinburg, 620990, Russia
[4]Mikheev Institute of Metal Physics UB RAS, 18 S. Kovalevskoy Str., Yekaterinburg, 620108, Russia

E-mail: sokovnin@iep.uran.ru

Abstract. The mesoporous nanocrystal powders BaF_2 and CaF_2 with a specific surface up to 34.8 and 88.7 sq.m/g, respectively, are produced by the pulsed electron beam evaporation method in vacuum. The influence of thermal annealing of nanoparticles on air in the range of temperature from 200 to 900°C on the size, morphology of particles and change of their magnetic and luminescent properties investigated have been investigared. The essential stoichiometric impurity (overage of metals) and significant growth in a specific surface of nanopowders (NP) BaF_2 and CaF_2 after annealing at the temperature of 200°C have been detected. It is established that the synthesized NP BaF_2 is a paramagnetic while initial material in the bulk state is diamagnetic. After annealing at 900°C appears the small ferromagnetic contribution at NP BaF_2. Produced NP CaF_2 showed ferromagnetic behavior. In literature there is no information about the ferromagnetism of CaF_2. Appearance of the ferromagnetic response can be explained with formation of structural and radiation defects (F-centers, etc.). The analysis of PCL and magnetization curves of samples BaF_2 and CaF_2 allows drawing conclusions about their connection.

1. Introduction

Nanofluorides of alkali earth metals have good prospects for use as catalysts and photonics materials, including precursors of optical ceramics and materials for biomedical applications [1]. Various methods for preparing CaF_2 nanoparticles are known, the first being chemical ones: the exposure of corresponding nanoscale oxides to gaseous hydrogen fluoride [2], chemical precipitation from solutions [3, 4], co-precipitation from acidic solutions of corresponding salts using a hydrogen fluoride solution with product crystallization in cubic syngony [5], thermolysis of alkali earth trifluoroacetates [6, 7] and others. Physical methods for producing fluoride nanopowders are less developed because their realization involves significant difficulties, e.g. the laser method [8].

The aim of the present work was to obtain nanopowders (NPs) of BaF_2 and CaF_2 using electron beam evaporation in a vacuum [9], and also to investigate the structural, morphological, magnetic, luminescent and textural properties of the obtained NPs.

2. Experimental technique

Targets from the BaF_2 micron powder of optical purity and CaF_2 (TU 6-09-2412-84) were pressed onto a manual press. The pellets were sintered in an electric furnace in air at a temperature of 900°C (without isothermal conditioning) on YSZ (Y_2O_3+10wt% ZrO_2) support and then they were cooled together with the furnace to room temperature. The settings were: evaporation mode on installation Nanobim-2 [9]: acceleration voltage – 38 kV; pulse duration – 100 μs; frequency – 50 pps; beam current – 0.2 A; the development area of the beam on the target surface – 8 cm^2; time of evaporation – 50 minutes; residual air pressure in the transpiration chamber – 4 Pa. The nanoparticles were deposited onto the support of ordinary glass of large area, 4 mm thick, positioned at a distance of 10-15 cm from the target center. The speed of evaporation of the target was 5.5 g/hour, collection of NPs reached 85% of the total mass of the evaporated CaF_2. Then, a portion of the produced BaF_2NP was annealed in alundum crucibles at the temperature 200°C, 400°C and 900°C within 10 min. Henceforth in this paper the CaF_2 NP samples, prior to and after annealing at the temperatures of 200, 400 and 900°C, will be designated as S0, S200, S400 and S900, respectively

The specific surface area (Sssa) of NPs was defined by the Brunauer-Emmet-Teller (BET) method on the Micromeritics TriStar 3000 installation. The crystal structures of the NPs and bulk samples were characterized by Shimadzu X-ray diffractometer XRD-7000 with nickel-filtered Cu in a 2θ range 20–90°. SEM images and EDX analysis were measured by scanning electron microscopes LEO982 with Oxford X-Ray Detector. The surface morphologies and sizes of the samples were observed by a JEOL (Japan) JEM 2100 Transmission Electron Microscope (TEM). The magnetization curves were measured by Faraday balance magnetometer. Temperature measurements were carried out in (Ar+H2) atmosphere. Photoluminescence (PL) spectra were recorded at room temperature using an MDR-204 device (deuterium lamp, R928 photoelectronic multiplier made by Hamamatsu). Pulse cathode luminescence (PCL) spectra were recorded using a KLAVI-1 device [10].

3. Results and discussion

The X-ray phase analysis has shown that NPs CaF_2 are single-phased and that there is only fluorite (PDF-2 map No. PDF-2 00-035-0816) and NPs BaF_2 have the cubic structure of frankdicksonite (PDF-2, card No. 00-004-0452 for BaF_2). The parameters of lattices for the starting and annealed NPs are outlined in table 1.

The texture analysis (table 1) has shown that isotherms of absorption/desorption of the S0 and S200 samples NPs BaF_2 and CaF_2 are related to the Type IV isotherms according to the IUPAC classification [11], which indicates the mesoporous NP type. Emergence of the hysteresis loop of the H-3 type demonstrates the formation of asymmetric, mutually connected slit-like mesoporousness in the samples. Significant growth in the specific area of the CaF_2 and BaF_2 NPs was found after annealing at the temperature of 200º C (Table 1). Annealing at 900 ºC has led to the growth in particle size, which is confirmed by the X-ray phase analysis data (a decrease in the half-width of diffraction peaks) and a loss of mesoporousness by the S900 sample BaF_2 and CaF_2.

The TEM and SEM results are shown in figure 1. Not annealed NPs BaF_2 and CaF_2 have typical form for this method NP producing [9] and consist of small aggregates of crystalline particles (figure 1a), combined to agglomerates. The SEM photographs demonstrate a change in morphology as a result of thermal annealing of samples especially agglomeration a sponge-like or coral-like shape in sample S200 (figure 1c). The EDX analysis data are represented in table 2.

Table 1. Crystallographic and texture properties of CaF_2 and BaF_2 NPs.

Sample	*a*, nm	FWHM	S_{BET}, (m^2/g)	$V_{p\text{-}otal}$(cm^3/g)	D_{BJH} (nm)
target (CaF_2)	-	-	18.5	0.127	24.9
S0 (CaF_2)	5.4606 (6)*	0.141 (1)	64.3	0.25	21
S200 (CaF_2)	5.4582 (5)	0.22 (3)	88.7	0.66	29
S900 (CaF_2)	5.4588 (6)	0.101 (4)	1.11	0.0025	37
S0 (BaF_2)	6.1917 (6)	0.22 (4)	19	0.46	29.3
S200 (BaF_2)	6.1914 (6)	0.35 (7)	34.8	0.31	30.1
S900 (BaF_2)	6.1933 (5)	0.108(18)	0.46	0.0092	160

*– measurement error in parentheses, FWHM – full width at half maximum; $V_{p\text{-}Total}$ – total pore volume, D_{BJH} – average pore diameter, S_{BET} – specific surface.

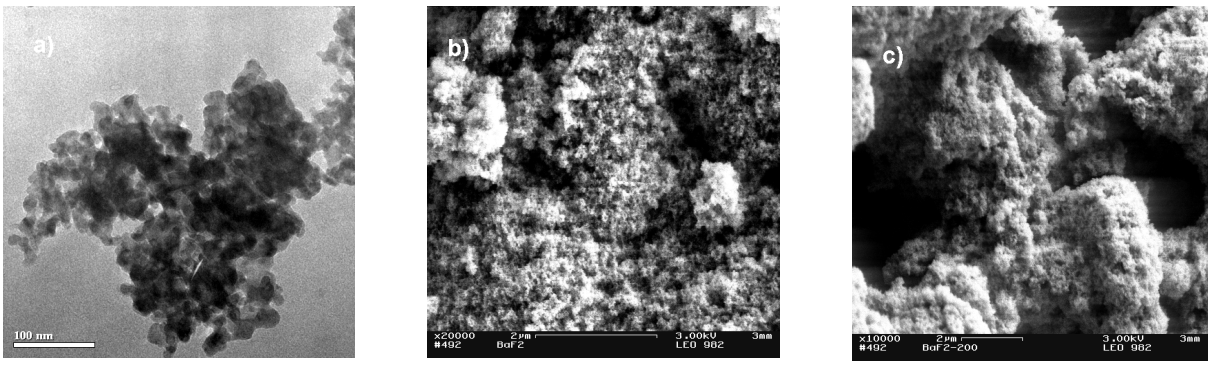

Figure 1. Morphology NP BaF_2: TEM of the sample S0, SEM of the samples S0(b), S200(c).

Table 2. Results of energy dispersion X-ray analysis (EDX).

Element	wt.%		at.%		Element	wt.%		at.%	
	S0	S200	S0	S200		S0	S200	S0	S200
BaF_2					**CaF_2**				
C	1.49	6.78	9.46	29.70	C	2.55	3.24	6.01	7.35
O	0.00	1.07	0.00	3.52	O	1.05	1.55	1.85	2.65
F	10.42	13.19	41.73	36.53	F	30.57	33.46	45.59	48.01
Ba	88.09	78.97	48.81	30.26	Ca	65.84	61.75	46.54	42.00

The EDX analysis data in table 2 indicate an absence of any magnetic impurities (Fe, Co and Ni) in the samples. The uniformly distributed impurity of carbon (as well as of oxygen) could have been adsorbed from the vacuum oil vapours in the evaporation chamber and environmental atmosphere during the collection and storage of samples. A strong distortion of stoichiometry in the samples should be noted: in both samples there is an excess of calcium, the concentration of which decreases after annealing.

The PL spectra for the CaF_2 samples are broad bands with maxima at λ_{max}~684 nm (table 3). Annealing of the samples at 200°C does not lead to a shift of λ_{max} (band excitation 320-380 nm). In the last case the band intensity is somewhat decreased. The luminescence is determined by the F-centers. After Gaussian decomposition two bands emerge, responsible for the two types of F-centers with maxima at ~650 (1 type) and ~702 nm (2 type) (samples prior to and after annealing) [11]. Distinct oxygen content in the samples indicates its participation in the formation of F-centers with a complex

structure [12]. After annealing, the PL intensity for both F-centers decreases 1.3- and 1.2-fold, respectively (table 3). This fact indicates a small decrease in the number of F-centers, apparently due to their partial recombination with possible hole centers of the V_k type formed during target evaporation [13, 14].

The PL spectra for the BaF_2 have at large the same structure. The PL spectrum of sample S0 represents a wide strip with a maximum at λ_{max}=680 nm; in sample S200 λ_{max}=672 nm. The annealing of sample S200 at 200°C led to an increase in the intensity of the red strip by 2.1 times. The luminescence is caused by the F-centers. After decomposition on gaussiana there are revealed two strips responsible for two types of F-centers with maxima at ~653 (1 type) and ~705 nm (2 type) (for the S0 sample) and at ~648 (1 type) and 700 nm (2 type) (for the S200 sample). The increase in the intensity of PL occurs because of an increase in the number of F-centers of the 1st type by ~3 times, of the 2nd type by ~4.3 times.

Table 3. Results of analysis of PL and PCL for samples.

Sample	A1, a.u.	λ1, nm	FWHM1, nm	A2, a.u.	λ2, nm	FWHM2, nm	A3, a.u.	λ3, nm	FWHM3, nm	A3/A2
PCL										
target	1331	502	48	1992	522	92	-	-	-	-
S0	702	498	50	602	532	114	240	637	229	0.4
S200	1242	497	64	799	544	101	586	627	275	0.73
S400	1426	499	65	1360	524	164	503	678	230	0.37
S900	236	486	154	727	673	120	872	713	138	1.2
FL										
S0	-	-	-	340634	650	50	389389	702	55,6	1.14
S200	-	-	-	255980	650	50	332402	701	57	1.3

The reduction of the issue intensity of sample S200 that was observed on the BaF_2 PCL spectra (figure 2a), in comparison with sample S0, may have been caused by the reduction in the size of particles as noted above. Annealing at 900°C, followed by growth in the size of particles, leads to significant growth in PCL. We note that the PCL intensity of sample S900 even exceeded the PCL intensity of micron size powder (bulk), confirming the data of X-ray phase analysis and the textural analysis of the S900 sample's exit from a nanostate. Changes in the crystallite size are also notably followed (~50 nm) by a red shift in the IR intensity maximum in samples S0 and S200.

The decrease in sample intensity observed in the CaF_2 PCL spectra (figure 2b) is not significant in view of the fact that the PCL yield is not normalized at the time of measurement. However, the alteration in the PCL spectrum is of a curious nature. After Gaussian decomposition three bands appear in the NPs (table 3), which are responsible for the two types of F-centers with maxima (maintaining the numbering introduced for PL) at ~500 (3 type), ~530 (4 type), ~630 (5 type), ~650 (1 type) and ~702 nm (2 type). These bands are a consequence of recombination processes.

In the PCL spectra, after annealing of the samples at 200 and 400°C, a broad band (FWHM ~230 nm) is observed at ~630 nm (table 3); this band is shifted 110-130 nm compared to the PCL spectra of the target, which have two adjacent peaks. While peaks 3 and 4 in the PCL spectra of the target and NP samples annealed at temperatures of 200 and 400º C nearly do not change at all, when taking into account approximation errors, peak 5 changes significantly at amplitude annealing (with respect to peak 4 of the spectrum, table 3), and maintains a larger width.

After annealing at 900°C, peak 3 decreases drastically, while peaks 4 and 5 almost disappear, merging into one broad band at ~650 nm; a new band appears at ~702 nm (table 3).

In our opinion, the centers, the number of which increases at annealing, are responsible for the bands at ~530 and ~630 nm. These bands may be caused by delocalization of hole centers and their recombination with F-centers [13]. The broad band at 702 nm is analogous to that in the PL spectrum.

Apparently, after annealing at 900° C during PCL, it is for the most part the same F-centers which are excited by radiation at 320-380 nm.

The initial unannealed CaF_2 NP (S0) has demonstrated ferromagnetic (FM) behavior (figure 3a) and NP BaF_2 (S0) demonstrated paramagnetic (PM) behavior (figure 3b). The literature has only fragmented data about ferromagnetism of CaF_2 and no information about paramagnetism BaF_2.

The emergence of the FM and PM response may be explained by the formation of structural and radiation defects (F-centers etc.), precisely for NP CaF_2 in the bands at ~530 and ~630 nm. A feature of the NPs obtained by the method used is the presence of a large number of structural defects of various types [8] as well as the targeting of an evaporating beam of electrons of radiation defects by deceleration radiation. Therefore, analogous to the model [15], it can be supposed that only fluoride vacancies somehow participate in the formation of FM and PM in the S0 and S200 samples.

Here, air annealing NP CaF_2 (S200 sample) has led to an increase in the FM contribution almost by an order of magnitude at simultaneous significant growth on PCL intensity in the bands at ~530 and ~630 nm, and also an alteration of their mutual intensity. This confirms the responsibility of these bands only for the defective nature of magnetism. Annealing at 900°C (the S900 sample), which leads to a significant increase in particle size (Table 1), has simultaneously led to the disappearance of the FM state and to an alteration in the structure of the PCL spectrum (table 3). Apparently, at such annealing all features of the structure (defect state), that emerged at synthesis of such NPs, disappear.

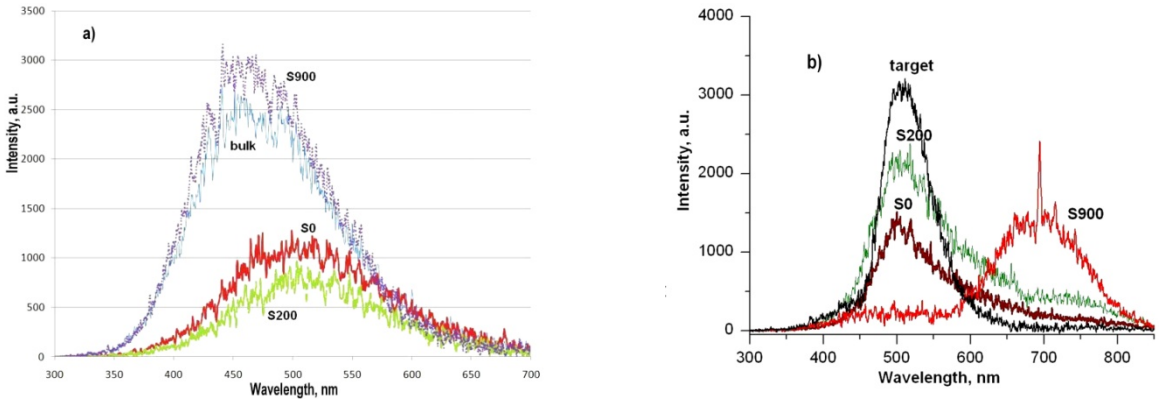

Figure 2. PLC spectra of samples BaF_2 (a) and CaF_2 (b) before and after annealing.

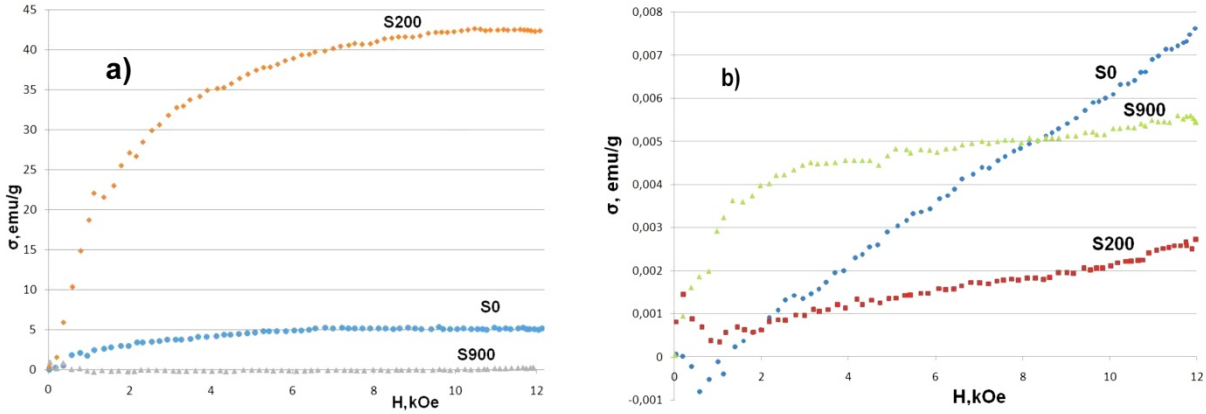

Figure 3. Magnetization curve of the samples CaF_2 (a) and BaF_2 (b) before and after annealing.

A decrease in the deficiency of samples, caused by a decrease in the number of anion (fluoride) vacancies resulting from the oxidation of excess barium, may be the mechanism for the decrease in magnetization in the case of annealing at 200°C. Annealing NP CaF_2 at 900° C (the S900 sample), which leads to a significant increase in particle size (table 1), has simultaneously led to the disappearance of the FM state and to an alteration in the structure of the PCL spectrum (table 3). Apparently, at such annealing all features of the structure (defect state), that emerged at synthesis of NP CaF_2.

4. Conclusion

Thus, mesoporous nanopowders of BaF_2 and CaF_2 were produced, with strong violation of stoichiometry due to an excess of metall. This study found the growth of the NP CaF_2 and BaF_2 specific surface after annealing at a temperature of 200°C and an increase in the intensity of the red strip NP BaF_2 by 2.1 times after annealing, due to an increase in the number of the F-centers of the 1st type in ~3 and of the 2nd type in ~4.3 times and also change of PCL spectrum of CaF_2 NP. The noticeable (~50 nm) red shift of a PCL intensity maximum in S0 and S200 samples NP BaF_2 was established. After annealing of the samples at a temperature 200°C and 400°C in PCL spectra of NP CaF_2 obtains the wide (FWHM ~230 nm) band at ~630nm, which is shifted for 110-130 nm as compared with PCL spectrum of the target.

For the first time PM behavior of the BaF_2 nanopowders and FM response at NP CaF_2 was found, which can be explained by the formation of structural and radiation defects during producing NP. The analysis of the PCL and magnetization curves of samples allows conclusions to be drawn on their connection.

PM is responsible for sample S0 BaF_2 decreasing after annealing at a temperature of 200°C, and at the same time for the PCL intensity of sample S200 BaF_2 also decreasing. The S0 sample of CaF_2 shows an FM response, which increases after annealing in air at a temperature of 200°C. Thereby, a significant growth in intensity of PCL of NP CaF_2 occurs in the bands at ~530 and ~630 nm, along with an alteration of their mutual intensity. Annealing at a temperature of 900°C has led to the disappearance not only of the FM response in the S900 sample of NP BaF_2 and CaF_2.

It is possible that the increase in FM in the CaF_2 NPs at annealing in an oxygen-containing medium occurs according to the mechanism similar to the one outlined in the papers [16–17], which involve oxygen vacancies (fluoride vacancies in our case). This requires further investigation.

Acknowledgments

The authors are grateful to Pryanichnikov S.V., a researcher of the shared equipment center "Ural" of the Institute of Metallurgy of the Ural division of RAS, for the X-ray phase analysis; to the researchers of the Institute of Electrophysics of the Ural division of RAS Demina T.M. for the texture analysis, Murzakayev A.M. and Timashenkova O.R. for the microscopic analysis, Spirina A.V. for the PCL analysis. This work has been carried out within the scope of government order No. 0389-2015-0026 and with partial support of RFBR project No. 18-08-00514. The magnetic measurements were carried out within the scope of government order under the topic MAGNIT, state registration No. AAAA-A18-118020290129-5.

References

[1] Patent RU 2619738 2017
[2] Patent RU 2328448 2008
[3] Alharbi N 2015 *J. of Nanomaterials* **2015** 136957
[4] Andrade A, Ferreira N and Valerio M 2017 *RSC Adv.* **7** 26839
[5] Kuznetsov S, Yarotskaya I, Fedorov P, Voronov V, Lavrishchev S, Basiev T and Osiko V 2007 *Russian J. of Inorganic Chem.* **52** 315
[6] Sathyamurthy S,Tuncer E, More K, Gu B, Sauers I and Paranthaman M 2012 *ApplPhys A.* **106** 661

[7] Osipov V, Lisenkov V, Platonov V and Tikhonov E 2018 *Quantum Electronics* **48** 235
[8] Sokovnin S and Il'ves V 2012 *J. Ferroelectrics* **436** 101
[9] Sokovnin S, Il'ves V and Zuev M 2016 *Engineering of Nanobiomaterials Applications of Nanobiomaterials* vol 2, ed A Grumezescu (Amsterdam: Elsevier) p 29
[10] Mesyats G, Michaylov S, Osipov V and Solomonov V 1992 *Tech. Phys. Lett.* **18** 87
[11] Glynn T 1991 *J. of Lumin.* **48–49** 783
[12] Salah N, Alharbi N, Habib S and Lochab S 2015 *J. of Nanomaterials* **2015** 136402
[13] Antonyak O, Vistovskyy V, Zhyshkovych A and Kravchuk I 2015 *J. Lumin.* **67** 249
[14] Figura P, Nepomnyaschich A and Radzhabov E 1988 *Optics and Spectroscopy* **65** 940
[15] Singhal R, Kumari, Samariya A, Kumar S, Sharma S, Xing Y and Saitovitch E 2010 *Appl. Phys. Lett.* **97** 172503
[16] Gao D, Yang Z, Zhang J, Yang G, Zhu Z, Qi J, Si M and Xue D 2011 *AIP Advances* **1** 042168
[17] Ahmed S, Viboon P, Ding X, Bao N, Du Y, Herng T, Ding J and Yi J 2018 *J. of Alloys and Compounds* **746** 399